Synthesis and Understanding the Role of Donor-Tetracyanobutadiene on Porphyrin β-Periphery Towards Ultrafast Charge Transfer Dynamics

Andrew W. Dawson,[a,≠] Bijesh Sekaran,[b,≠] Somnath Das,[a] Rajneesh Misra,*[a] Francis D'Souza*[b]

[a]Department of Chemistry, University of North Texas, 1155 Union Circle, #305070, Denton, TX 76203-5017, USA.

E-mail: Francis.DSouza@UNT.edu

[b]Department of Chemistry, Indian Institute of Technology, Indore 453552, India.

E-mail: rajneeshmisra@iiti.ac.in

[≠]Equal contribution

Abstract

The porphyrins, structurally analogous to chlorophyll pigment, have drawn significant interest in mimicking natural photosynthetic processes in energy conversion applications. In this work, a new set of β-substituted free-base (H_2P) and zinc-porphyrins (ZnP) have been designed (**5-19**) and synthesized employing ferrocene (Fe), triphenylamine (TPA) and carbazole (Cz) as secondary donors (D) and further incorporated tetracyanobuta-1,3-diene (TCBD) as strong electron acceptor (A) entity following Sonogashira cross-coupling and subsequent [2+2] cycloaddition-retroelectrocyclization reactions. Steady-state optical data exhibits a broad absorption in the 650-800 nm region, particularly in **15-19**, corroborating ground-state charge polarization leading to intramolecular charge transfer (CT) in these systems. Strong fluorescence quenching in all the systems (**5-19**) compared to the control compounds (**C1** and **C2**) further suggests excited state nonradiative photo-processes predominate in these β-substituted dyads and triads, particularly after TCBD incorporations (**15-19**). Though the secondary donors quickly oxidize in **5-10**, the same becomes difficult in **15-19**, indicating an electronic influence of TCBD, leading to the respective formation of $MP^{\bullet-}$-$D^{\bullet+}$ and $MP^{\bullet+}$-$A^{\bullet-}$-D (MP = 2H or Zn) charge separated (CS) species in a polar environment, which the molecular orbital positioning of the CT entities from computational studies has also justified. Finally, spectral and temporal dynamics of different photo products in these compounds have been assessed from femtosecond transient absorption studies, and subsequent fitting of the transient data identifies Cz contributing to the most stable and thus long-lived CS states, brightening their outstanding promise in solar energy harvesting and related electronic applications.

Introduction

The art of solar energy harvesting is, and has been, a popular topic of discussion for advancing the future of renewable energy sources.[1-4] In this line, organic artificial photosynthetic systems have recently been at the forefront of photoinduced electron transfer (PET) studies as promising solar energy harvesting chromophores.[5-12] At their very core, these systems are primarily comprised of covalently bonded (sometimes pi-conjugated) electron-rich donors (D) and electron-deficient acceptor (A) entities that interact with one another, leading to PET in the excited state following photoexcitation.[13-24] Subsequently, in the excited state, one of the solvent-stabilized interactions can occur, facilitating the formation of the charge-separated (CS) states involving the generation of radical ion pairs before recombination, leading to deactivation to the ground state. The ability to modify and exploit the CS state and the subsequent charge recombination of a push-pull system is vital for developing solar energy harvesting devices with higher levels of solar-energy conversion efficiencies.

Various configurations of light-harvesting organic push-pull systems have been synthesized and studied.[5-51] However, one of great interest and particular focus has recently been on porphyrin-based systems owing to their facile synthetic methodologies and excellent redox activities.[5, 11, 34-51] Porphyrin-based systems can also be easily tuned to speed up electron transfer and slow down the charge recombination process, which is ideal for solar energy harvesting systems.[50] This can be achieved by introducing additional covalently bound electron acceptor and donor species to the metal-containing (MP) or free-base porphyrin (H_2P) porphyrins.[34-40, 47-49] By changing and pairing the electron donating and accepting groups of different strengths with the MP and H_2P, the goal is to increase the pi-conjugation and, thus, extend the electronic absorptions of push-pull systems for enhanced solar energy absorption in developing more efficient light-harvesting devices, specifically for the dye-sensitized solar cells.[5-12, 52] Along this note, we have recently reported excited state electrochemical and photophysical dynamics, including intramolecular charge transfer (CT) characteristics of a range of porphyrin-based push-pull systems (**1-4**, **11-14**, and **C1-C2** shown in Figure 1) with phenothiazine (PTZ) and N,N-dimethylaniline (NND) as secondary donors and tetracyanobutadiene (TCBD) as an acceptor and established CT/CS processes involving the D/A entities.[34]

In the present work, we have gone a step further, based on our previous study,[34] and herein expanded our research horizon by developing new porphyrin-based D-A systems of a range of new secondary donors of variable donicity (**5-10**) along with their TCBD analogs (**15-19**)**,** shown in Figure 1 (dashed box) and, thereby, report a comprehensive photo-electro-chemical response of these compounds. Apart from the porphyrin core as the primary donor in all the compounds, three peripheral electron-rich entities, namely ferrocene (Fc, compounds **5-6** and **15-16**), triphenylamine (TPA, compounds **7-8** and **17-18**), and carbazole (Cz, compounds **9-10** and **19**) have been introduced as secondary donors and then strategically incorporated TCBD as a strong electron

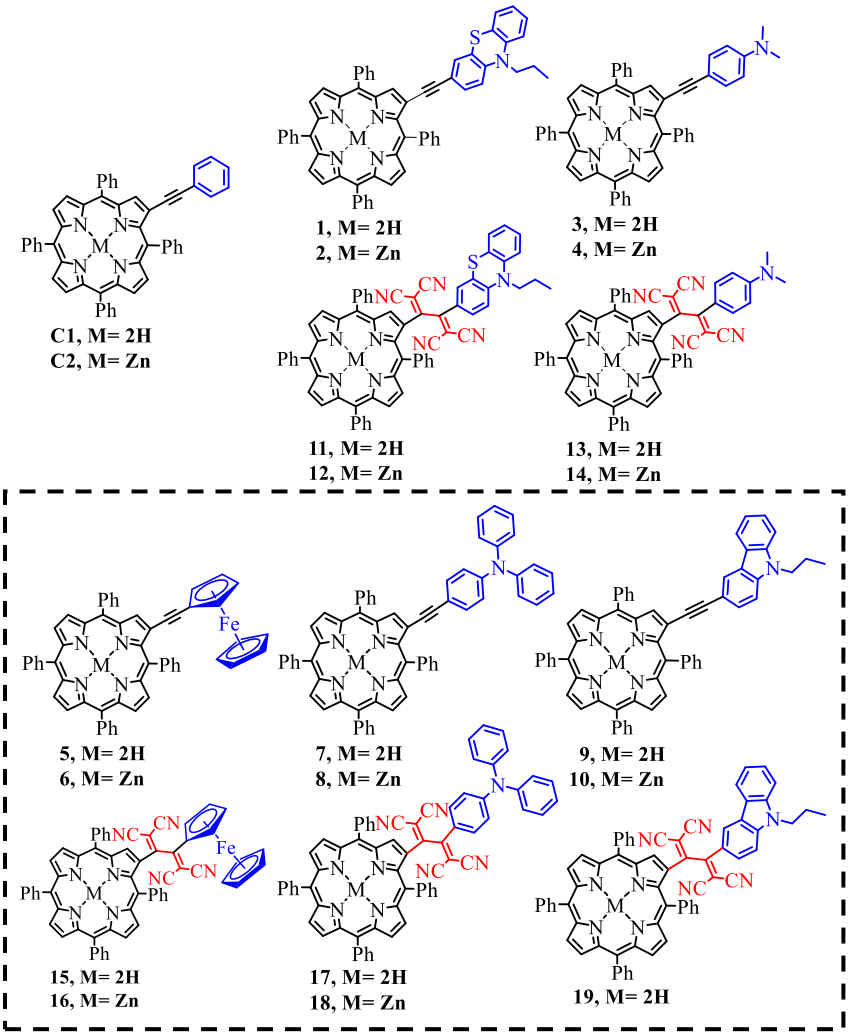

Figure 1. *Structure of the investigated MP-D and MP-A-D (MP = 2H or Zn, Donor = PTZ, NND, Fc, TPA, or Cz) conjugates and the two control compounds (**C1** and **C2**). Compounds **C1**, **C2**, **1-4,** and **11-14** have been previously published[34] and shown here to comprehensively understand the presently investigated MP-A-D push-pull systems (**5-19**) shown in the dashed box.*

acceptor following Sonogashira cross-coupling[49] and subsequently [2+2] cycloaddition-retroelectrocyclization (CA-RE) reactions.[53] The origin of the new broad low-energy absorption feature and strong quenching of fluorescence suggests effective nonradiative intramolecular CT, particularly in TCBD embedded samples (**15-19**), leading to energetically feasible $MP^{\bullet-}$-$D^{\bullet+}$ and $MP^{\bullet+}$-$A^{\bullet-}$-D types (MP = 2H or Zn) of CS states related to compounds **5-10** and **15-19**, respectively. While electrochemical data assess the feasibility of CT processes, theoretical calculations further identify the molecular orbitals involved in low-energy CT (and subsequent CS) events in these MP-D and MP-A-D molecules. Finally, femtosecond transient absorption (fs-TA) studies provided the spectral signature of the evolved photo-excited species and their associated lifetimes, discerning Cz-based compounds with better CT/CS stabilization and thus longer lifetimes, making them coveted for energy conversion technologies.

Materials and Methods

All chemicals were used as received unless otherwise noted. All moisture-sensitive reactions were performed under an argon/nitrogen atmosphere. The NMR spectra were recorded at room temperature (298 K). Chemical shifts are given in ppm with respect to tetramethylsilane as the internal standard ($CDCl_3$, 7.26 ppm, 77.0 ppm). ^1H NMR and ^{13}C NMR spectra were recorded using a 400 MHz and 100 MHz spectrometer. The density functional theory (DFT) calculations were carried out at the B3LYP/6-31G level for C, N, H, O, and Zn in the Gaussian 09 program. HRMS was recorded on the TOF-Q mass spectrometer.

The UV-visible spectral measurements were carried out with a Shimadzu Model 2550 double monochromator UV-visible spectrophotometer. The fluorescence emission was monitored using a Horiba Yvon Nanolog coupled with time-correlated single photon counting with nanoLED excitation of 494 nm diode laser. A right-angle detection method was used. Differential pulse and cyclic voltammograms were recorded on an EG&G PARSTAT electrochemical analyzer using a three-electrode system. A platinum button electrode was used as the working electrode. A platinum wire served as the counter electrode, and an Ag/AgCl electrode was used as the reference electrode. Ferrocene/ferrocenium redox couple was used as an internal standard. A supporting electrolyte solution of 0.1 M $(TBA)ClO_4$ in DCB was used for all electrochemical studies. All the solutions were purged before electrochemical and spectral measurements using argon gas.

Spectroelectrochemical studies were performed using a cell assembly (SEC-C) supplied by ALS Co., Ltd. (Tokyo, Japan). This assembly comprised a Pt counter electrode, a 6 mm Pt Gauze working electrode, and an Ag/AgCl reference electrode in a 1.0 mm path length quartz cell. The optical transmission was limited to 6 mm, covering the Pt Gauze working electrode. Spectra were recorded by applying a potential 80 mV past the potential of a given oxidation or reduction process and continued until no additional changes were observed. A supporting electrolyte solution of 0.2 M (TBA)ClO_4 in DCB was used for all spectroelectrochemical studies.

Femtosecond transient absorption spectroscopy experiments were performed using an ultrafast femtosecond laser source (Libra) by Coherent incorporating a diode-pumped, modelocked Ti:sapphire laser (Vitesse) and a diode-pumped intracavity doubled Nd:YLF laser (Evolution) to generate a compressed laser output of 1.45 W. A Helios transient absorption spectrometer coupled with a femtosecond harmonics generator, provided by Ultrafast Systems LLC, was used for optical detection. The sources for the pump and probe pulses were derived from the fundamental output of Libra (Compressed output 1.45 W, pulse width 100 fs) at a repetition rate of 1 kHz; 95% of the fundamental output of the laser was introduced into a TOPAS-Prime-OPA system with a 290−2600 nm tuning range from Altos Photonics Inc., (Bozeman, MT), while the rest of the output was used for generation of a white light continuum. Kinetic traces at appropriate wavelengths were assembled from the time-resolved spectral data. Data analysis was performed using Surface Xplorer software supplied by Ultrafast Systems. All measurements were conducted in degassed solutions at 298 K. The estimated error in the reported rate constants is ±10%.

Synthetic Details

Synthesis of compound 5. 7-bromo-5,10,15,20-tetraphenylporphyrin **20** (0.120 g, 0.173 mmol), ethynyl ferrocene **22** (0.054 g, 0.260 mmol) in THF: TEA (1: 1, v/v), palladium(0)-tetrakis(triphenylphosphine) (0.070 g, 0.06 mmol), and CuI (0.005 g, 0.025 mmol) were added under argon atm at room temperature. The reaction mixture was stirred for 12 h at 70 °C, and then cooled to room temperature. The solvent was then evaporated under reduced pressure, and the resultant mixture was diluted with DCM, and the organic layer was collected, dried over anhydrous Na_2SO_4, and evaporated under vacuum. The solid was adsorbed on silica gel and purified by column chromatography, using a DCM: hexane (20: 80) mixture to produce (0.100 g, 70%) of compound **5**.^{1}H NMR (400 MHz, $CDCl_3$): δ ppm= 9.00(s, 1 H), 8.85(s, 2 H), 8.81(d, 1 H), 8.77(s,

2 H), 8.71(d, 1 H), 8.25–8.20(m, 8 H), 7.88–7.77(m, 12 H), 4.36(s, 2 H), 4.25(s, 7 H), -2.68(s, 2 H). ^{13}C NMR (101 MHz, $CDCl_3$) : δ ppm= 142.32, 142.13, 141.88, 141.64, 135.05, 128.30, 127.81, 127.75, 126.78, 126.74, 126.68, 126.62, 120.51, 120.00, 119.93, 119.58, 98.82, 82.44, 72.30, 69.90, 68.81, 65.96. HRMS (ESI-TOF): m/z calculated for $C_{56}H_{38}FeN_4$ $[M]^+$ 822.2442, found 822.2483.

Synthesis of compound 6. Compound **5** (0.100 g, 0.121 mmol), Zn $(OAc)_2$, (0.266 g, 1.21 mmol) in MeOH: $CHCl_3$ (3: 1, v/v) were added, and the reaction mixture was stirred for 1 h at room temperature. The solvent was then evaporated under reduced pressure, and the resultant mixture was diluted with DCM/water. The organic layer was collected, dried over anhydrous Na_2SO_4, and evaporated under vacuum. The solid was adsorbed on silica gel and purified by column chromatography, using a DCM: hexane (35: 65) mixture to produce (0.095 g, 90%) of compound **6**. ^{1}H NMR (400 MHz, $CDCl_3$) : δ ppm= 9.17(s, 1 H), 8.90(m, 4 H), 8.87(d, 1 H), 8.75(d, 1 H), 8.25–8.20(m, 8 H), 7.80–7.76(m, 12 H), 4.39(s, 2 H), 4.26(s, 7 H). ^{13}C NMR (101 MHz, $CDCl_3$) : δ ppm= 142.91, 142.77, 141.80, 137.95, 135.69, 135.22, 135.00, 134.88, 134.42, 134.33, 133.11, 132.19, 131.66, 127.52, 126.75, 126.63, 126.59, 126.55, 126.38, 125.05, 123.25, 113.21, 110.61, 72.34, 70.57, 69.92. HRMS (ESI-TOF): m/z calculated for $C_{56}H_{36}FeN_4Zn$ $[M]^+$ 884.1577, found 884.1565.

Synthesis of compound 15. Compound **5** (.050 g, 0.060 mmol) and tetracyanoethylene **21** (.019 g, 0.152 mmol) were dissolved in 7 ml 1,2-dichloroethane. The mixture was stirred overnight at room temperature. The resultant mixture was poured into water and extracted with dichloromethane. After drying over Na_2SO_4, the remaining liquid was concentrated and purified by column chromatography using (hexanes: dichloromethane=40: 60) to produce (.052 g, 91%) of compound **15**. ^{1}H NMR (400 MHz, $CDCl_3$): δ ppm= 8.97(s, 1 H), 8.85(s, 2 H), 8.72(d, 2 H), 8.65(d, 2 H), 8.35(s, 4 H), 8.17(s, 4 H), 7.85–7.77(m, 12 H), 4.81(s, 2 H), 4.49(s, 2 H), 4.17(s, 5 H), -2.20(s, 2 H). ^{13}C NMR (101 MHz, $CDCl_3$): δ ppm= 141.52, 141.25, 140.78, 140.54, 140.04, 138.26, 135.71, 134.90, 134.72, 134.58, 134.42, 132.80, 130.70, 130.08, 129.43, 129.12, 128.65, 128.26, 127.95, 127.10, 126.89, 126.77, 124.60, 120.57, 120.29, 114.44, 113.89, 112.35, 74.33, 73.86, 71.92. HRMS (ESI-TOF): m/z calculated for $C_{62}H_{38}FeN_8$ $[M+nH]^+$ 951.2643, found 951.2638.

Synthesis of compound 16. Compound **6** (.050 g, 0.056 mmol) and tetracyanoethylene **21** (.018 g, 0.141 mmol) were dissolved in 7 ml 1,2-dichloroethane. The mixture was stirred overnight at room temperature. The resultant mixture was poured into water and extracted with dichloromethane. After drying over Na_2SO_4, the remaining liquid was concentrated and purified by column chromatography using (hexanes: dichloromethane=10: 90) to produce (.047 g, 82%) of compound **16**. ^{1}H NMR (500 MHz, $CDCl_3$): δ ppm= 9.08(s, 1 H), 8.93–8.91(d, 1 H), 8.84–8.79(dd, 2 H), 8.73–8.69(dd, 2 H), 8.64(s, 1 H), 8.34–8.13(m, 7 H), 8.02(d, 1H), 7.78–7.70(m, 12 H), 4.81(s, 2 H), 4.62(s, 2 H), 4.19(s, 5 H). ^{13}C NMR: Repeated attempts did not result in quality spectrum. HRMS (ESI-TOF) m/z: calculated for $C_{62}H_{36}FeN_8Zn$ $[M+nNa]^+$ 1035.1596, found 1035.1597.

Synthesis of compound 7. 7-bromo-5,10,15,20-tetraphenylporphyrin **20** (0.120 g, 0.173 mmol), 4-ethynyl-N,N-diphenylaniline **23** (0.070 g, 0.260 mmol) in THF: TEA (1: 1, v/v), palladium(0)-tetrakis(triphenylphosphine) (0.070 g, 0.06 mmol), and CuI (0.005 g, 0.025 mmol) were added under argon atm at room temperature. The reaction mixture was stirred for 12 h at 70 °C and then cooled to room temperature. The solvent was then evaporated under reduced pressure, the resultant mixture was diluted with DCM, and the organic layer was collected, dried over anhydrous Na_2SO_4, and evaporated under vacuum. The solid was adsorbed on silica gel and purified by column chromatography, using a DCM: hexane (20: 80) mixture to produce (0.100 g, 66%) of compound **7**. ^{1}H NMR (500 MHz, $CDCl_3$) : δ ppm= 9.03(s, 1 H), 8.86(s, 2 H), 8.81(d, 1 H), 8.77(s, 2 H), 8.71(d, 1 H), 8.22– 8.19(m, 8 H), 7.79–7.69(m, 12 H), 7.31(t, 4 H), 7.21(d, 2 H), 7.16(d, 4 H), 7.09(t, 2 H), 7.00(d, 2 H), -2.68(s, 2 H). ^{13}C NMR (126 MHz, $CDCl_3$) : δ ppm= 137.83, 134.57, 134.53, 133.13, 129.41, 129.00, 128.46, 127.77, 126.79, 126.75, 126.69, 125.03, 123.49, 121.91. HRMS (ESI-TOF): m/z calculated for $C_{64}H_{43}N_5$ $[M+nH]^+$ 882.3591, found 882.3634.

Synthesis of compound 8. Compound **7** (0.100 g, 0.113 mmol), Zn $(OAc)_2$, (0.248 g, 1.13 mmol) in MeOH: $CHCl_3$ (3 : 1, v/v) were added, and the reaction mixture was stirred for 1 h at room temperature. The solvent was then evaporated under reduced pressure, and the resultant mixture was diluted with DCM/water, and the organic layer was collected, dried over anhydrous Na_2SO_4 and evaporated under vacuum. The solid was adsorbed on silica gel and purified by column chromatography, using a DCM: hexane (35: 65) mixture to produce (0.095 g, 90%) of compound **8**. ^{1}H NMR (500 MHz, $CDCl_3$) : δ ppm= 9.19(s, 1 H), 8.91(d, 4 H), 8.86(d, 1 H), 8.75(d, 1 H), 8.22–8.19(m, 8 H), 7.79–7.71(m, 9 H), 7.70–7.68(m, 3 H), 7.31(t, 4 H), 7.24(d, 2 H), 7.16(d, 4 H),

7.09(t, 2 H), 7.01(d, 2 H). ^{13}C NMR (126 MHz, $CDCl_3$) : δ ppm= 150.71, 150.55, 147.35, 142.71, 138.61, 134.40, 134.31, 133.15, 132.20, 129.40, 127.53, 126.60, 126.50, 124.99, 123.46, 121.98. HRMS (ESI-TOF) m/z: calculated for $C_{64}H_{41}N_5Zn$ $[M]^+$ 943.2648, found 943.2691.

Synthesis of compound 17. Compound **7** (.050 g, 0.056 mmol) and tetracyanoethylene **21** (.018 g, 0.141 mmol) were dissolved in 7 ml 1,2-dichloroethane. The mixture was stirred overnight at room temperature. The resultant mixture was poured into water and extracted with dichloromethane. After drying over Na_2SO_4, the remaining liquid was concentrated and purified by column chromatography using (hexanes: dichloromethane=40: 60) to produce (.051 g, 90%) of compound **17**. ^{1}H NMR (500 MHz, $CDCl_3$) : δ ppm= 8.88(d, 1 H), 8.79(d, 1 H), 8.76(s, 1 H), 8.73(d, 1 H), 8.70(d, 1 H), 8.61–8.58(dd, 2 H), 8.30(s, 2 H), 8.23(d, 2 H), 8.14–8.11(m, 4 H), 7.76–7.75(m, 3 H), 7.72–7.69(m, 6 H), 7.68–7.66 (m, 3 H), 7.25(t, 4 H), 7.12–7.09(m, 2 H), 7.07 (d, 4 H), 6.94 (d, 2 H), 6.86 (d, 2 H), -2.38(s, 2 H). ^{13}C NMR: After repeated submission, peaks were not raised. HRMS (ESI-TOF) m/z: calculated for $C_{70}H_{43}N_9$ $[M+nH]^+$ 1010.3714, found 1010.3719.

Synthesis of compound 18. Compound **8** (.050 g, 0.053 mmol) and tetracyanoethylene **21** (.016 g, 0.132 mmol) were dissolved in 7 ml 1,2-dichloroethane. The mixture was stirred overnight at room temperature. The resultant mixture was poured into water and extracted with dichloromethane. After drying over Na_2SO_4, the remaining liquid was concentrated and purified by column chromatography using (hexanes: dichloromethane=20: 80) to produce (.052 g, 90%) of compound **18**. ^{1}H NMR (500 MHz, $CDCl_3$): δ ppm= 8.96(s, 1 H), 8.81(d, 1 H), 8.77–8.74(m, 3 H), 8.68(d, 1 H), 8.51(d, 1 H), 8.21(m, 4 H), 8.11(d, 4 H), 7.74–7.63(m, 12 H), 7.31(t, 4 H), 7.19–7.13(m, 6 H), 6.96–6.89(m, 4 H). ^{13}C NMR (126 MHz, $CDCl_3$) : δ ppm= 153.21, 152.46, 152.32, 151.64, 149.98, 145.73, 142.70, 134.56, 134.47, 133.61, 133.16, 133.10, 132.87, 132.64, 132.52, 129.87, 129.53, 129.14, 127.97, 127.62, 126.76, 126.66, 126.49, 125.59, 119.76, 114.40, 110.55. HRMS (ESI-TOF) m/z: calculated for $C_{70}H_{41}N_9Zn$ $[M+nNa]^+$ 1094.2669, found 1094.2792.

Synthesis of compound 9. 7-bromo-5,10,15,20-tetraphenylporphyrin **20** (0.120 g, 0.173 mmol), 3-ethynyl-9-propyl-9H-carbazole **24** (0.060 g, 0.260 mmol) in THF: TEA (1: 1, v/v), palladium(0)-tetrakis(triphenylphosphine) (0.070 g, 0.06 mmol), and CuI (0.005 g, 0.025 mmol) were added under argon atm at room temperature. The reaction mixture was stirred for 12 h at 70 °C, and then cooled to room temperature. The solvent was then evaporated under reduced pressure, and the

resultant mixture was diluted with DCM and the organic layer was collected, dried over anhydrous Na_2SO_4 and evaporated under vacuum. The solid was adsorbed on silica gel and purified by column chromatography, using a DCM: hexane (20: 80) mixture to produce (0.105 g, 72%) of compound **9**. ^{1}H NMR (500 MHz, $CDCl_3$) : δ ppm= 9.10 (s, 1H), 8.87(s, 2H), 8.82(d, 1 H), 8.78(s, 2 H), 8.74(d, 1 H), 8.29(d, 2 H), 8.25–8.24(m, 2 H), 8.22–8.17(m, 5 H), 8.10(s, 1 H), 7.81– 7.73(m, 12 H), 7.52(t, 1 H), 7.48–7.44(dd, 2 H), 7.37–7.30(m, 2 H), 4.30(t, 2 H), 1.97(m, 2 H), 1.04–1.01(t, 3 H), -2.65(s, 2 H). ^{13}C NMR (126 MHz, $CDCl_3$) : δ ppm= 142.26, 142.15, 142.00, 141.89, 141.45, 140.90, 140.04, 134.66, 134.61, 134.58, 134.53, 129.86, 128.57, 127.75, 126.83, 126.78, 126.74, 126.68, 126.00, 124.88, 122.67, 122.53, 120.46, 120.15, 120.01, 119.80, 119.33, 108.99, 108.26, 44.81, 22.37, 11.85. HRMS (ESI-TOF): m/z calculated for $C_{61}H_{43}N_5$ $[M+nH]^+$ 846.3591, found 846.3583.

Synthesis of compound 10. Compound **9** (0.100 g, 0.118 mmol), Zn $(OAc)_2$, (0.258 g, 1.18 mmol) in MeOH: $CHCl_3$ (3 : 1, v/v) were added, and the reaction mixture was stirred for 1 h at room temperature. The solvent was then evaporated under reduced pressure, and the resultant mixture was diluted with DCM/water, and the organic layer was collected, dried over anhydrous Na_2SO_4 and evaporated under vacuum. The solid was adsorbed on silica gel and purified by column chromatography, using a DCM: hexane (35: 65) mixture to produce (0.090 g, 84%) of compound **10**. ^{1}H NMR (500 MHz, $CDCl_3$) : δ ppm= 9.26(s, 1H), 8.93(s, 2H), 8.91(s, 2H), 8.88(d, 1H), 8.78(d, 1H), 8.28–8.24(m, 4H), 8.22–8.18(m, 5H), 8.12(s, 1H), 7.81– 7.72(m, 12H), 7.53–7.49(m, 2H), 7.45(d, 1H), 7.37(d, 1H), 7.32(t, 1H), 4.31(t, 2H), 1.99–1.95(m, 2H), 1.03(t, 3H). ^{13}C NMR (126 MHz, $CDCl_3$): δ ppm= 151.20, 150.67, 150.50, 150.17, 148.61, 146.30, 142.73, 142.30, 140.90, 140.01, 138.48, 134.43, 132.73, 132.20, 131.68, 129.90, 128.40, 127.60, 127.53, 126.87, 126.59, 125.98, 124.89, 122.69, 122.53, 121.48, 121.12, 120.98, 120.66, 120.46, 119.31, 108.25, 44.82, 29.71, 22.39, 14.13, 11.86. HRMS (ESI-TOF): m/z calculated for $C_{61}H_{41}N_5Zn$ $[M]^+$ 907.2648, found 907.2677.

Synthesis of compound 19. Compound **9** (0.050g, 0.059 mmol) and tetracyanoethylene **21** (.018 g, 0.147 mmol) were dissolved in 7 ml 1,2-dichloroethane. The mixture was stirred overnight at room temperature. The resultant mixture was poured into water and extracted with dichloromethane. After drying over Na_2SO_4, the remaining liquid was concentrated and purified by column chromatography using (hexanes: dichloromethane=40: 60) to produce (.053 g, 92%) of

compound **19**. ^{1}H NMR (500 MHz, $CDCl_3$) : δ ppm= 8.90(d, 1H), 8.88(s, 1H), 8.81(d, 1H), 8.72(d, 1H), 8.68(d, 1H), 8.62–8.58(dd, 2H), 8.27(m, 4H), 8.14(d, 4H), 8.00 (d, 1H), 7.83(s, 1H), 7.78–7.77(m, 3H), 7.73–7.66(m, 8H), 7.56(s, 1H), 7.46(t, 1H), 7.36(t, 2H), 7.32–7.30(m, 1H), 7.23(t, 1H), 4.20(t, 2H), 1.86–1.81(m, 2H), 0.90(t, 3H), -2.37(s, 2H). ^{13}C NMR (126 MHz, $CDCl_3$): δ ppm= 144.79, 143.07, 142.42, 141.89, 141.29, 138.95, 135.48, 134.98, 134.88, 134.78, 134.66, 132.74, 128.60, 128.00, 127.60, 127.51, 127.18, 127.12, 126.99, 126.90, 126.46, 126.38, 125.78, 125.72, 125.64, 123.27, 123.21, 122.76, 121.06, 120.50, 109.63, 45.30, 22.27, 11.75. HRMS (ESI-TOF): m/z calculated for $C_{67}H_{43}N_9$ $[M+nH]^+$ 974.3714, found 974.3745.

Results and Discussion

The *β*-donor substituted porphyrin and its zinc complex **5**, **6**, **7**, **8**, **9,** and **10** undergoes [2 + 2] CARE reaction with 2.5 equiv of TCNE in dichloroethane (DCE), resulting in *β*-substituted TCBD functionalized porphyrins **15**, **16**, **17**, **18**, and **19** in 91, 82, 90, 90, 92, and 90% yields, respectively. The porphyrin derivatives **5**-**10** and **15**-**19** were characterized by ^{1}H and ^{13}C NMR and HR-MS spectra (Figures S1-S31; see supporting information for details).

The synthesis of donor-substituted TCBD functionalized *β*-pyrrolic porphyrins **5**-**10** and **15**-**19** are depicted in Scheme 1. The *β*-monobrominated tetraphenyl porphyrin (TPPBr) **20** and *β*-donor substituted porphyrins **5**, **6**, **7**, **8**, **9,** and **10** were synthesized according to the reported procedures (Scheme 1).[53-55] The TPPBr **20** undergoes Sonogashira cross-coupling reaction with 1.5 equiv. of ethynyl ferrocene **22**, 4-ethynyl-N,N-diphenylaniline **23**, 3-ethynyl-9-propyl-9H-carbazole **24**, in THF: TEA (1:1) mixture, in the presence of $Pd(PPh_3)_4$ at 70 °C resulted in porphyrin **5**, **7,** and **9** in 70, 66, and 72% yield, respectively (Scheme 1). The zinc metallation on *β*-substituted ferrocenyl porphyrin **5** was carried out using $Zn(OAc)_2{\cdot}2H_2O$ by dissolving in MeOH and $CHCl_3$ (3:1) mixture, which resulted in zinc complexes **6** with 90% yield. The donor (Fe, TPA, and Cz) substituted TCBD functionalized *β*-pyrrolic porphyrins **15**, **16**, **17**, **18**, and **19** were synthesized by [2 + 2] CA-RE reaction and are shown in Scheme 1.

Optical Studies

The steady-state absorption studies of the secondary donor-substituted TCBD-functionalized β-porphyrins **5**-**10**, and **15**-**19**, were conducted in benzonitrile at room temperature, and the resulting

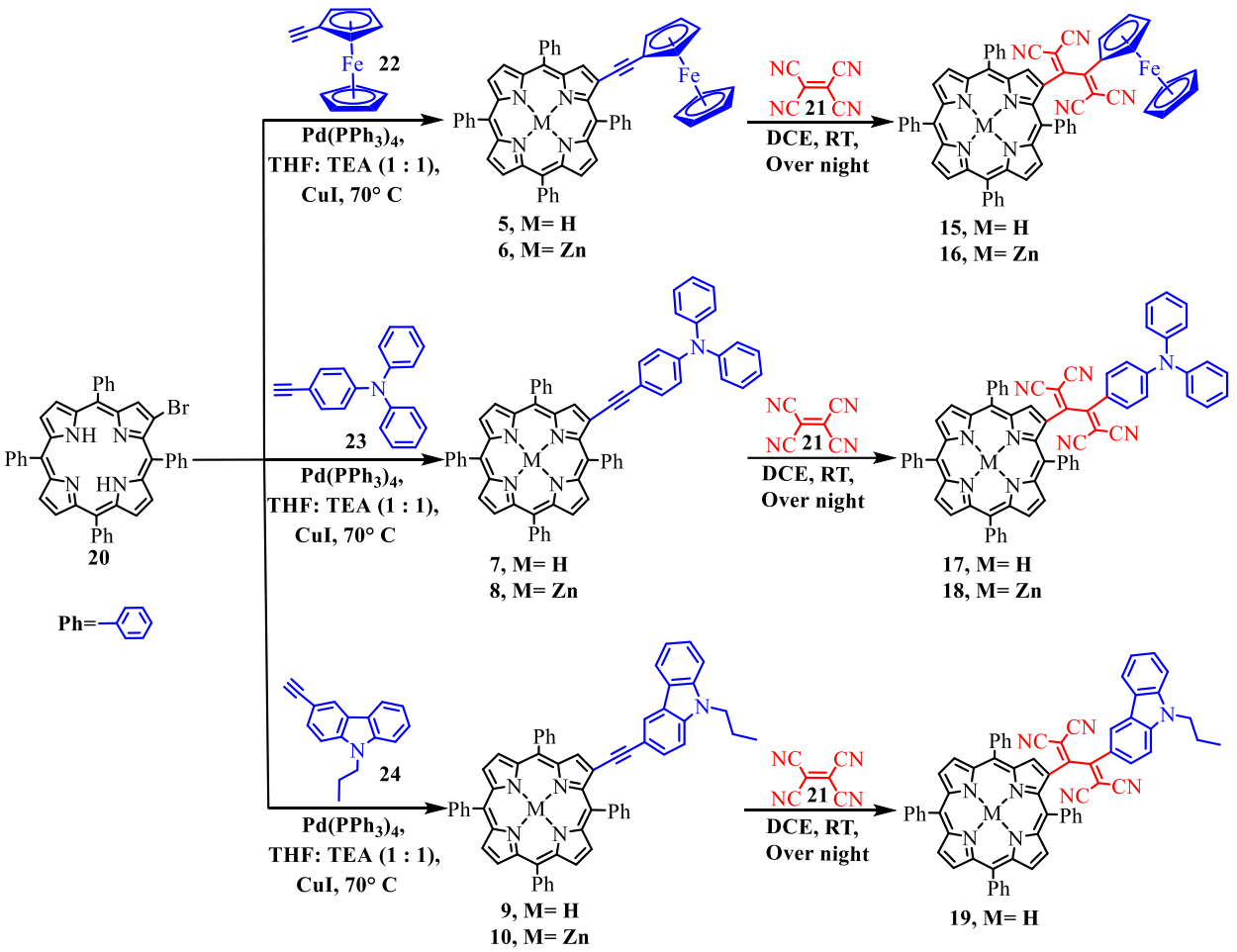

Synthesis Scheme 1. *Synthetic routes designed for β-pyrrole push-pull porphyrins* ***5****–****10*** *and* ***15****–****19***.

optical data is summarized in Table 1. The porphyrins (H_2P and ZnP) show characteristic intense Soret band absorptions in the 415-445 nm region and Q-bands in the 500-700 nm window. The first row in Figure 2 illustrates the absorption spectra of H_2P compounds (**5**, **7**, **9**, **15**, **17**, and **19**), while the first row of Figure S32 shows the corresponding ZnP compounds (**6**, **8**, **10**, **16**, and **18**), with and without the TCBD acceptor. Interestingly, the H_2P compounds (**5**, **7**, and **9**) show the characteristic Soret band along with four observable Q-band absorptions, whereas the ZnP derivatives (**6**, **8**, and **10**) exhibit the same characteristic Soret band absorption with only two Q-bands in the visible region owing to electronic influence induced by Zn and also consistent with our previous observation.[46, 56, 34] A bathochromic shift of ~ 10 nm was seen for the Soret and visible Q-bands upon the introduction of the electron-accepting TCBD at the *β*-pyrrole site in, both the

H_2P (**15**, **17**, and **19**) and ZnP (**16** and **18**), indicating electronic interaction between the electron-rich and deficient entities in these compounds (Figure 2 and S32). The red-shifted absorptions in the donor-substituted TCBD-functionalized porphyrins (**15-19**) are due to the charge polarization induced by the electron-deficient TCBD unit with extended π-conjugation, leading to intramolecular CT in these systems between the donors and strong TCBD acceptors.[57] The low-lying broad absorption spanning in the ~ 600-800 nm region in **15-19** unambiguously

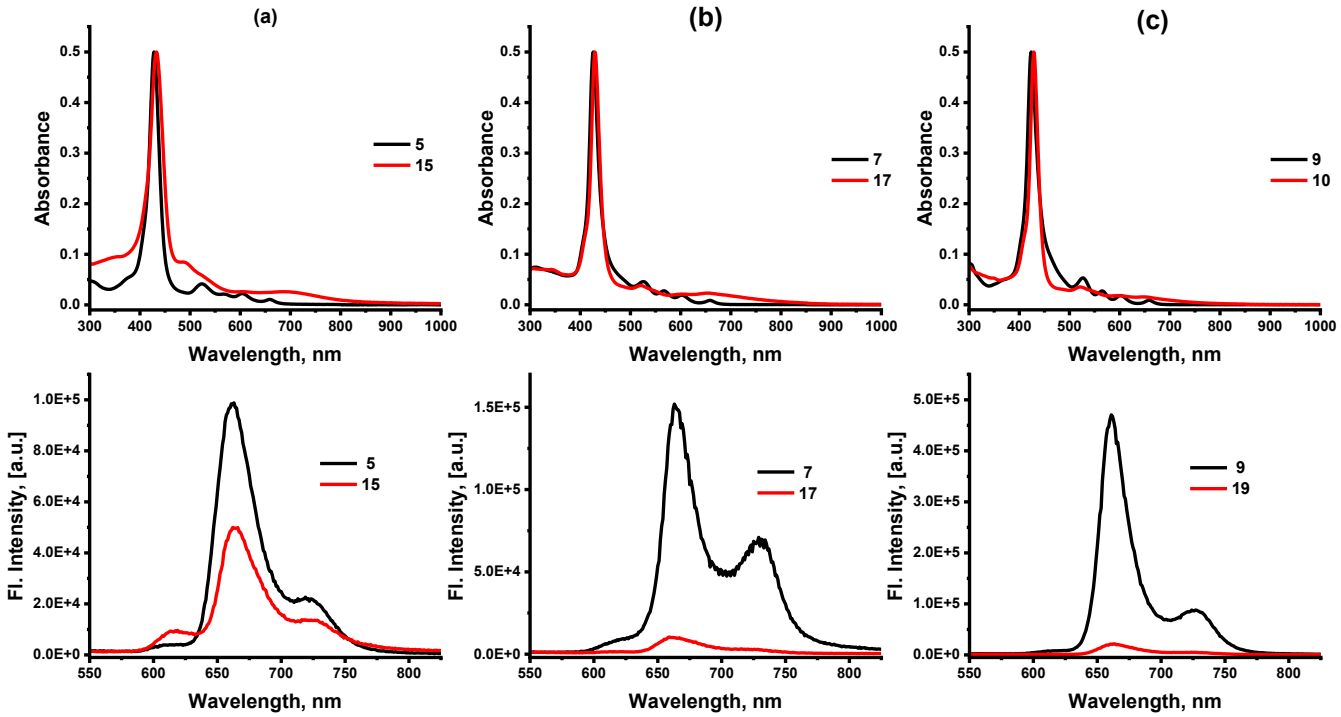

Figure 2. *Steady-state absorption (top row) and fluorescence (bottom row) spectra of (a)* ***5*** *and* ***15****, (b)* ***7*** *and* ***17****, and (c)* ***9*** *and* ***19*** *in benzonitrile. The samples were excited at the respective Soret peak maxima for all the compounds.*

suggests CT phenomena in these compounds after TCBD incorporation. Note that these observations are consistent with our previous report[34] for **1-4** and **11-14**, and thus, inevitably, intramolecular CT operates in the ground state of MP-A-D constructs involving TCBD acceptor.

The bottom row of Figure 2 illustrates the fluorescence spectra of the H_2P systems (**5**, **7**, **9**, **15**, **17**, and **19**), while the ZnP complexes (**6**, **8**, **10**, **16**, and **18**) are illustrated in the bottom row of Figure S32. Upon Soret band excitation, the β-substituted porphyrins exhibited the characteristic two emission bands peaking at 650 and 740 nm for the H_2P compounds (Figure 2) and 600 and

670 nm for the ZnP complexes (Figure S32). Interestingly, incorporating TCBD significantly quenches the fluorescence in all compounds **15-19**, suggesting ICT-mediated effective non-radiative deactivation processes predominate in MP-A-D systems (Figure 2 and S32). For example, in the case of compounds **15**, **17**, and **19**, ~ 49, 93, and 95% of fluorescence quenching could be observed when compared with their respective TCBD-free counterparts (**5**, **7**, and **9**). A similar trend could also be observed in the case of ZnP samples exhibiting ~ 90-98% quenching after TCBD incorporation (Figure S32). It is also important to mention that no new emission

Table 1. *Absorption and fluorescence spectral data of the investigated compounds in benzonitrile. The values of the control compounds (**C1** and **C2**) have been collected from our previous work.*[34]

Compound	λ_{abs}, nm					λ_{Em}, nm		ϵ, $10^4 M^{-1}cm^{-1}$	τ_{Fl}, ns
C1	430	520	561	600	658	664	727	--	8.73
C2	440	566	607	--	--	620	670	--	1.78
5	428	524	568	604	659	662	722	11.15	6.78
6	437	526	571	607	--	618	661	1.85	1.58
15	433	486	528	604	690	672	724	1.23	--
16	435	515	564	604	660	618	665	5.70	--
7	426	526	567	603	659	663	727	6.88	7.69
8	439	531	571	607	660	621	673	6.98	1.71
17	429	521	549	602	653	667	721	1.49	--
18	438	567	607	677	--	620	670	10.00	--
9	424	526	565	602	659	663	728	5.00	8.74
10	440	530	570	606	662	620	671	0.97	1.74
19	429	521	550	598	649	657	714	4.03	--

corresponding to the CT state of the compounds **15**-**19** could be seen after excitation related to the CT absorption, further supporting strong non-radiative CT transitions in these compounds and entirely in line with TCBD-based compounds exhibiting ICT characteristics.[7-10, 33-40] It is, however, important to mention here that the fluorescence intensity of the compounds containing secondary donors (**5**-**10**) also significantly reduces with respect to that of the **C1** and **C2**, indicating excited

state nonradiative processes also take place in the MP-D systems even in the absence of TCBD entities (Figure S33).

Insights into the excited state dynamic processes of both H_2P and ZnP, as well as their TCBD-incorporated samples (**5-10, 15-19**, respectively), were obtained from their fluorescence lifetime measurements using time-correlated single photon counting (TCSPC) techniques having a time resolution of ~ 200 ps.[10, 49] The lifetimes of the H_2P samples (**5**, **7**, and **9**) were found to be 6.78, 7.69, and 8.74 ns, respectively, while that of the ZnP complexes (**6**, **8**, and **10**) exhibited lifetimes of 1.58, 1.71, and 1.74 ns, respectively (Figure S34 and Table 1). The ZnP systems exhibited a lower lifetime than their analogous H_2P compounds due to the heavy atom effect of Zn facilitating intersystem crossing, leading to quenched fluorescence and reduced lifetimes upon metalation.[46] However, due to extremely weak emission, the lifetimes for the MP-A-D conjugates (**15-19**) could not be obtained here. This further suggests that non-radiative excited state occurrences predominate in the MP-A-D systems owing to ICT transitions, which significantly impact the excited state processes of MP-A-D samples after insertion of the TCBD acceptor. Note that, compared to **C1** and **C2**, a faster fluorescence decay (i.e., shorter lifetime) of the MP-D systems (**5**-**10**) and subsequently even faster (immeasurable in our TCSPC setup) for the MP-A-D compounds (**15**-**19**) are found to be entirely in line with the observed trends in steady state fluorescence quenching of these samples. All data related to steady-state and time-resolved optical studies have been summarized in Table 1 for all MP-D and MP-A-D porphyrins (**5**-**10** and **15**-**19**), along with the associated control compounds (**C1** and **C2**).

Electrochemical Studies

To understand the feasibility of ICT processes, we have subsequently looked into the electrochemical responses of the compounds using both differential pulse voltammetry (DPV) and cyclic voltammetric (CV) techniques. It has been established that H_2P and ZnP reveal two one-electron oxidations and reductions.[48] Preliminary electrochemical studies suggest **C1** exhibits oxidation potentials of 0.47 and 0.72 V vs. Fc/Fc^+, while **C2** displays oxidation potentials of 0.30 and 0.62 V. Additionally, reduction potentials were found to be at -1.58 and -1.86 for **C1**, while that of -1.79 and -1.90 V in the case of **C2**.[34] Having additional redox-active entities linked to the porphyrin macrocycle is expected, showing additional oxidation and reduction peaks as the secondary donors could affect oxidation potentials, while the TCBD entity is likely to appear in

the reduction side.[33, 57] Figures 3a and 3b illustrate the DPV plots of MP-D and MP-A-D, respectively, in DCB containing 0.1 M (TBA)ClO_4 as supporting electrolyte, while the redox potentials are tabulated in Table 2. The tabulated data shows that ZnP was easier to oxidize than the H_2P *β*-pyrrole functionalized porphyrins (Figure 3a). Additionally, the DPV plots in Figure 3 show additional oxidation and reduction redox peaks corresponding to the secondary donors and TCBD acceptor. Inclusion of the secondary donor entities (Fc, TPA, and Cz) exhibits additional oxidation peaks in the MP-D systems (**5**-**10**), while the TCBD entity shows two one-electron

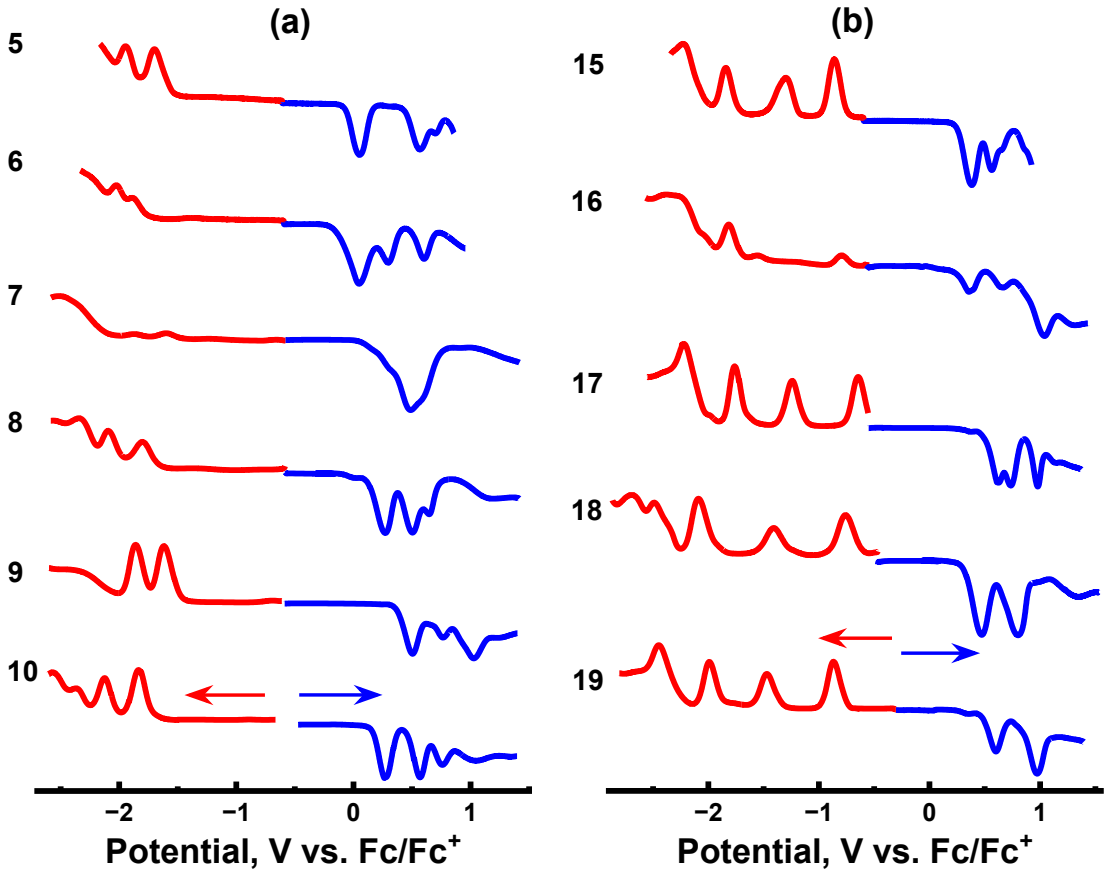

Figure 3. *DPVs of the indicated compounds in DCB containing 0.1 M (TBA)ClO_4. Scan rate = 5 m V/s, pulse width = 0.25 s, pulse height = 0.025 V. The potentials were referenced against the internal ferrocene/ferrocenium (Fc/Fc^+) redox couple.*

reductions, as can be visualized in Figure 3b. Comparing the redox potentials of **C1** and **C2**, we can predict the primary site of electron transfer in the H_2P- and ZnP-based systems containing secondary donors and TCBD acceptors. Notably, the first oxidation potential in **5**-**10** and **15**-**19** was due to the one-electron oxidation of the secondary donor entities (i.e., $D/D^{\bullet+}$), while the second

and third oxidation potentials were due to the MP core representing the $MP/MP^{\bullet+}$ and $MP^{\bullet+}/MP^{2+}$ species. The reversibility of these redox processes can also be judged from CV traces of the compounds (Figure S35).

***Table 2**. Experimental redox potentials and free-energy change for CT, CS, and CR of the investigated compounds in benzonitrile.*

Compound	Potential V vs. Fc/Fc^{+}							$E_{o,o}$, eV	E_{CT}, eV	ΔG_{sol}, eV	$-\Delta G_{CS}$, eV	$-\Delta G_{CR}$, eV
	E_{red}					E_{ox}						
	MP	MP	TCBD	TCBD	D	MP-D	MP-D					
C1	-1.86	-1.59	--	--	--	0.48	0.72	--	--	--	--	--
C2	--	-1.79	--	--	--	0.30	0.62	--	--	--	--	--
5	-1.95	-1.70	--	--	0.05	0.57	0.70	1.88	1.75	-0.336	0.46	1.42
6	-2.03	-1.89	--	--	0.05	0.30	0.60	2.02	1.94	-0.336	0.42	1.60
15	--	-1.84	-1.30	-0.86	0.38	0.56	0.66	1.82	1.24	-0.499	1.08	0.74
16	--	-1.82	-1.56	-0.79	0.36	0.66	1.04	1.94	1.15	-0.529	1.32	0.62
7	-1.87	-1.60	--	--	0.30	0.49	0.64	1.88	1.90	-0.226	0.20	1.67
8	-2.10	-1.80	--	--	0.27	0.51	0.65	1.94	2.08	-0.226	0.09	1.85
17	--	-1.76	-1.24	-0.65	0.63	0.74	0.98	1.88	1.27	-0.334	0.94	0.94
18	--	-2.09	-1.41	-0.76	0.47	0.80	0.98	1.91	1.23	-0.335	1.02	0.90
9	-1.86	-1.61	--	--	0.49	0.77	1.03	1.88	2.11	-0.232	0.00	1.88
10	-2.13	-1.84	--	--	0.28	0.57	0.76	1.93	2.12	-0.229	0.05	1.89
19	--	-1.99	-1.47	-0.87	0.60	0.83	0.97	1.90	1.47	-0.343	0.77	1.13

Similarly, incorporating the strong electron-accepting moiety, TCBD, resulted in two additional one-electron reversible reduction peaks in **15-19**, as shown in Figure 3b, and the corresponding CV traces are shown in Figure S35. These two additional one-electron reduction peaks result from the $TCBD^{0/\bullet-}$ and $TCBD^{\bullet-/2-}$ processes in these MP-A-D systems (**15-19**). Note that the lower oxidation potential of the secondary donors in **5-10** indicates their involvement in excited state electronic transitions, which in turn increases in **15-19** due to strong electronic influence of the TCBD acceptor, making them more challenging to oxidize in the presence of TCBD and, thus, less likely to be involved in ICT processes. From this electrochemical data, it can be concluded that the presence of the secondary donors and incorporation of TCBD acceptors strongly influences the redox properties of MP in MP-D and MP-A-D. We further performed computational studies, as discussed below, to elucidate the moieties involved in ICT and related excited state events.

Computational Studies and Energy Calculations

Subsequently, computational studies were carried out for molecular orbital visualization and energy calculation of the photo-generated species; therefore, ground state optimizations were performed using the B3LYP/6-31G* level of theory.[58] Figures 4 and S36 show the optimized structure, electrostatic potential energy maps, and frontier highest occupied molecular orbital (HOMO), HOMO-1, lowest unoccupied molecular orbital (LUMO), and LUMO+1 of the investigated MP-D and MP-A-D compounds with their corresponding energy values. As can be seen in Figure 4, in the MP-D systems (**5**, **7**, and **9**), the HOMO mainly extended across both the secondary donors and the porphyrin core, while the LUMO was primarily focused on the porphyrin ring. This suggests the possible formation of $MP^{\bullet-}$-$D^{\bullet+}$ type CS species upon photoinduced electron transfer involving the porphyrin core as the electron acceptor. Interestingly, after TCBD incorporation in the case of MP-A-D systems (**15**, **17**, and **19**), the HOMO was found to be centered solely on the porphyrin, while the LUMO was primarily identified on the electron-accepting TCBD entity with slight contributions from the porphyrin core only in **15** (Figure 4). The porphyrin center as HOMO and the change in the location of LUMO on TCBD suggests the formation of $MP^{\bullet+}$-$A^{\bullet-}$-D CS state during electron transfer between the MP donor and TCBD acceptor. As proximity of TCBD caused the oxidation of the secondary donors to be more complex, the MP entity acts as the predominate donor instead in **15**-**19**, as also evident from their HOMO delocalizations. It is also important to mention that the HOMO-1 state of compounds **15**, **17**, and **19** are localized on the secondary donors. Hence, their partial involvement in ICT transitions with TCBD acceptors cannot be ruled out.

Figure S36 shows that a similar trend can also be observed across ZnP-D and ZnP-A-D complexes. As expected, HOMO of the ZnP-D systems (**6**, **8**, and **10**) was found to be spread across both the secondary donor and the porphyrin core, while the LUMO was primarily centered on the porphyrin ring, indicating the formation of $ZnP^{\bullet-}$-$D^{\bullet+}$ type CS state upon photoexcitation, similar to that of their H_2P analogs in Figure 4. On the other hand, in ZnP-A-D compounds (**16** and **18**), the HOMO was solely on the porphyrin core, while the LUMO was primarily centered on the TCBD acceptors with little electron density visualized on the ZnP core. Thus, a similar $ZnP^{\bullet+}$-$A^{\bullet-}$-D CS state could be envisioned between the ZnP donor and TCBD acceptor in **16** and **18**, in line with their H_2P counterparts as discussed earlier. Computed frontier orbital energies for all optimized structures in the gas phase were summarized in Table S1.

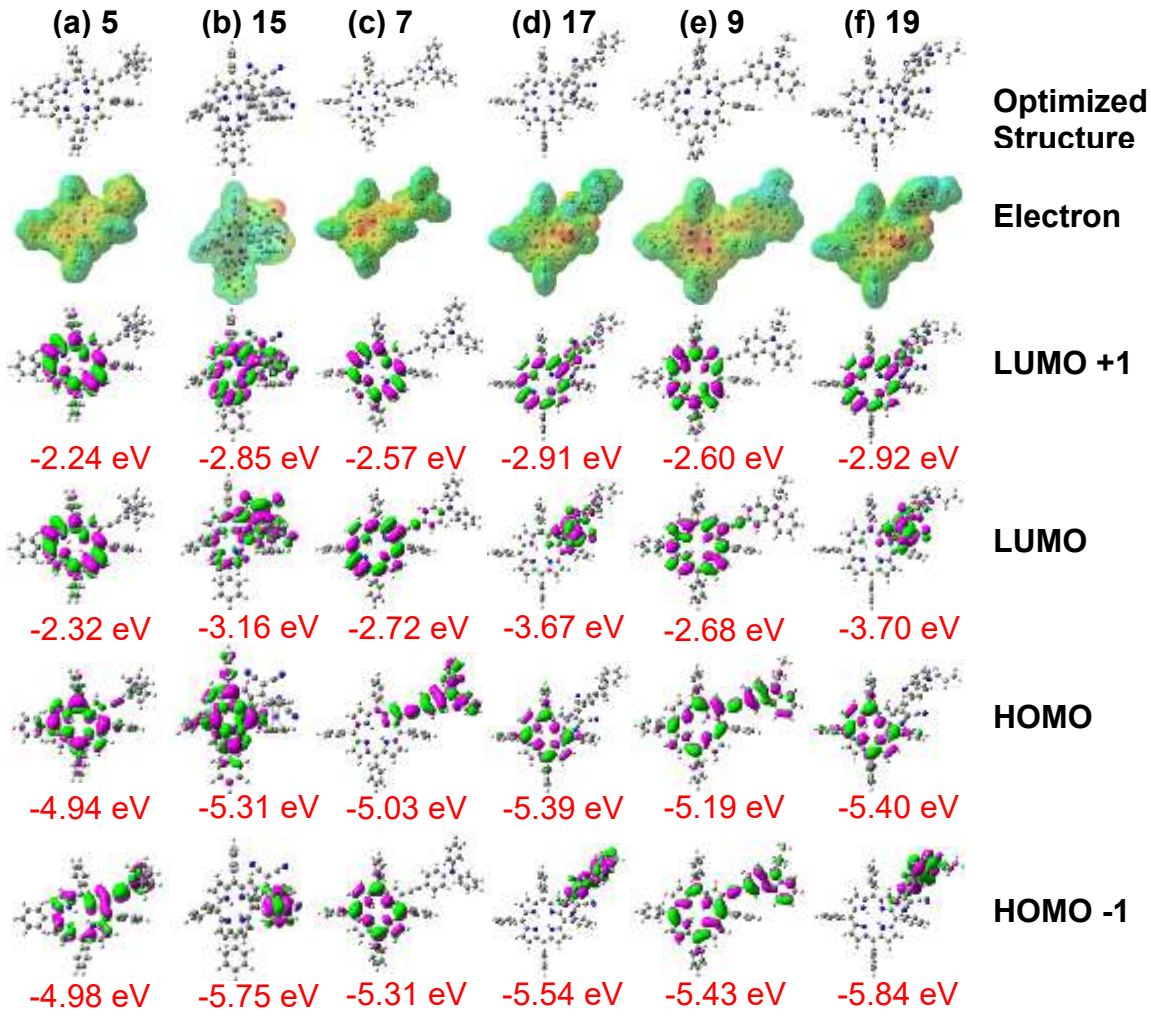

Figure 4. *B3LYP/6-31G* optimized structure, electrostatic potential energy maps, and frontier HOMO-1, HOMO, LUMO, and LUMO+1 of the indicated H_2Ps with and without TCBD.*

Subsequently, to find out the relaxation pathways of the photoinduced excited state species, the driving forces of the charge separation ($-\Delta G_{CS}$) and charge recombination ($-\Delta G_{CR}$) processes were first calculated using theoretical and the beforementioned optical and electrochemical data following equations 1 and 2 (Eq. 1 and 2) following the Rehm and Weller approach:[59]

$$-\Delta G_{CR} = E_{ox} - E_{red} + \Delta G_{Sol} \qquad \textbf{(Eq. 1)}$$

$$-\Delta G_{CS} = \Delta E_{0,0} - (-\Delta E_{CR}) \qquad \textbf{(Eq. 2)}$$

where, E_{ox} is the first oxidation potential of the donor (the Donor entity in both the MP-D and MP-A-D systems), E_{red} is the first reduction potential (the MP in the MP-D system, and the TCBD entity in the MP-A-D system), $\Delta E_{0,0}$ is the energy of the 0-0 electronic transition between the lowest vibrational states in the absorption and fluorescence peaks i.e. $\Delta E_{0,0}$ corresponds to singlet

energy of the compounds. The ΔG_{Sol} is a reference to the static energy, calculated by using the 'Dielectric Continuum Model' according to equation 3 (Eq. 3):

$$\Delta G_{Sol} = -e^2/(4 \cdot \pi \cdot \varepsilon_0 \cdot \varepsilon_s \cdot R_{Ct-Ct}) \qquad \textbf{(Eq. 3)}$$

where ε_0 represents vacuum permittivity (8.85 x 10^{-12} $C^2/N \cdot m^2$), and ε_s represents the dielectric constant of the utilized solvent, in our case, benzonitrile ($\varepsilon_s = 26$). The calculated values of different energy states, including the singlet, CT, and CS, have been presented in Table 2.

Energy Level Diagrams

The constructed energy level diagram below clearly allows us to visualize different photoinduced events in the MP-D and MP-A-D systems upon calculation of the energy of the excited state species based on the above Rehm and Weller equations and optical/electrochemical observations. As summarized in Figure 5, for both the MP-D and MP-A-D systems, photoexcitation corresponding to the higher energy Soret band initially forms a higher-lying singlet excited state (in this case is denoted by the S_2 state), which relaxes to the low-lying singlet excited ^{1}MP*-D state (S_1) *via* internal conversion (IC). In the case of the MP-D systems (**5-10**, Figure 5a), after IC from S_2 to S_1 state, energetically feasible $MP^{\bullet-}$-$D^{\bullet+}$ charge separated (CS) state emerges, which was likely stabilized by polar media, in this case benzonitrile. Considering energetics illustrated in Figure 5a, CS states subsequently undergo charge recombination (CR), forming the ^{3}MP-D* triplet excited states before complete deactivation to the ground state. Note that the direct formation of ^{3}MP-D* triplets is although energetically feasible from ^{1}MP*-D; however, considering HOMO-LUMO distribution and based on the computational data, CS states of ~ 1.42-1.89 eV energy likely corroborates the first CS, particularly in polar solvents before CR to the triplets in MP-D systems as schematically represented in Figure 5a.

In the case of the MP-A-D systems (**15-19**), incorporation of the TCBD entities causes facile charge polarization in the ground state (as seen in optical data) involving the TCBD acceptor, leading to easy formation of the $MP^{\delta+}$-$A^{\delta-}$-D CT states from the initially excited singlet states, as shown in Figure 5b. The CT states subsequently lead to solvent-stabilized $MP^{\bullet+}$-$A^{\bullet-}$-D CS states before CR to the ground state. Note that singlet-to-triplet ISC is also possible in these systems; however, considering energetics, singlet-to-direct CT transitions are energetically more feasible, and a lower CS lifetime (*vide infra*) further suggests non-involvement of triplets in the sequential deactivation pathways of the photoproducts in these MP-A-D compounds.

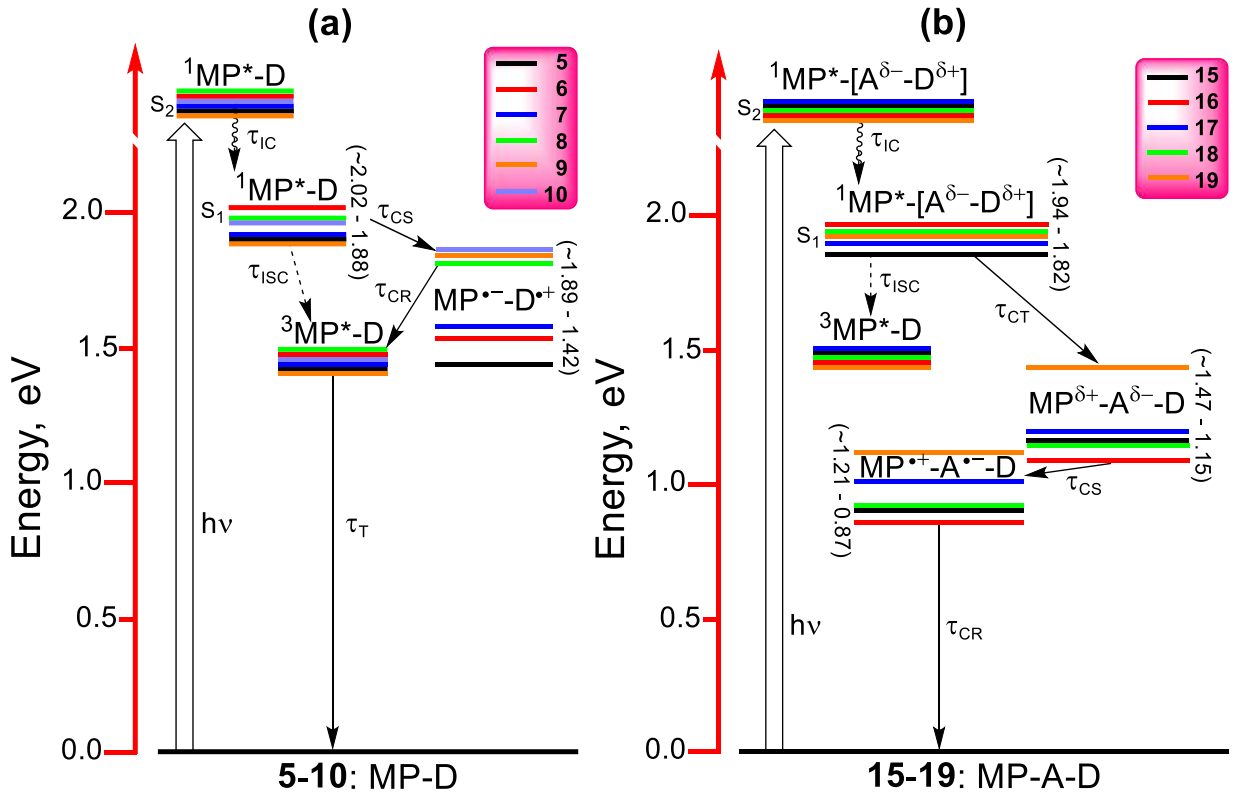

Figure 5. *Energy level diagrams depicting different photo-events in the (a) MP-D and (b) MP-A-D systems (MP = H_2P or ZnP, A = TCBD, Donor = Fe, TPA, and Cz). The energy of the charge transfer states in (b) are estimated from the charge transfer absorption bands shown in Figures 2 and S32.*

Femtosecond transient absorption pump-probe studies

To properly assess the spectral and kinetic information of the processes mentioned above in these MP-D and MP-A-D systems, femtosecond transient absorption (fs-TA) spectroscopy was implemented by excitation corresponding to the Soret band of each compound. Furthermore, to provide a comprehensive understanding, fs-TA responses of these compounds have also been compared to spectroelectrochemical and TA data of the control compounds, **C1** and **C2**, documented in our previous report.[34]

Figure 6 (left) shows the fs-TA spectra at the indicated delay times of H_2P-D (**5**, **7**, and **9**) in benzonitrile, while the corresponding ZnP-D (**6**, **8**, and **10**) spectra are shown in the left column of Figure S37. Upon photoexcitation related to the Soret band, the singlet state of the compounds initially appears according to the constructed energy profile diagram of the compounds. For example, at a shorter time delay, the instantaneously formed singlet of **5** (i.e., ^{1}**5***) revealed positive

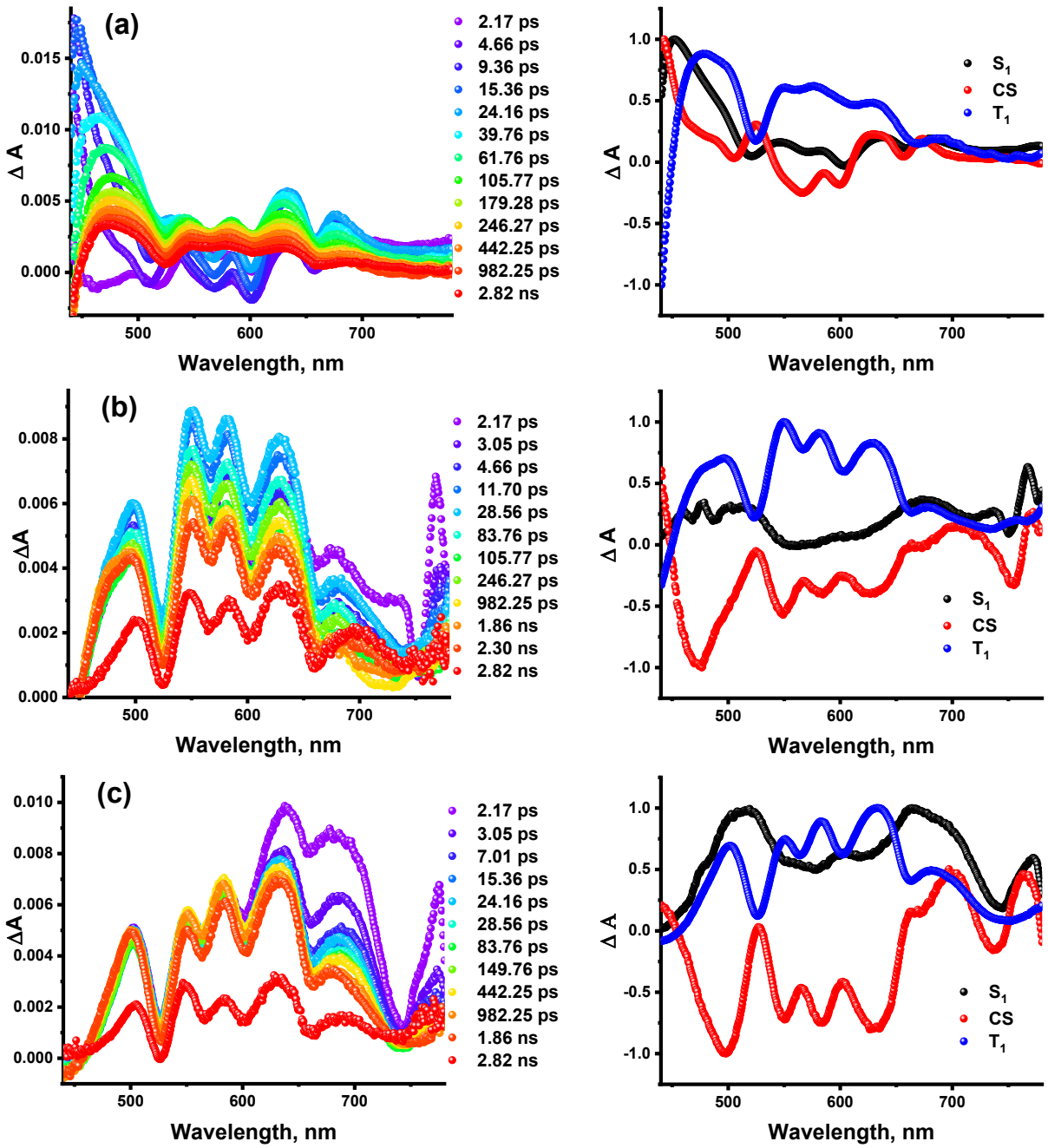

Figure 6. *Fs-TA spectra at the indicated delay times of (a)* ***5****, (b)* ***7****, and (c)* ***9*** *in benzonitrile (λ_{ex} = 426 nm) (left column). The DAS obtained from Target analysis are shown in the right column of the respective compounds.*

excited state absorption (ESA) peaks at 495, 545, 582, 634, and 688 nm, along with multiple characteristic negative signals at 462, 519, 567, 603, and 661 nm (Figure 6a) (see the fs-TA spectra

of 2.17 ps delay time). Considering the steady-state absorption and fluorescence data presented above, the first three negative signals can be assigned as the ground state bleach (GSB) whereas the latter two resulted from stimulated emission (SE) of **5**. Interestingly, the observed decay and recovery of these GSB and ESA signals of **5** are faster than those observed for **C1** in our previous report,[34] suggesting the ultrafast formation of the $MP^{\bullet-}$-$D^{\bullet+}$ CS state from the initially formed singlet. A similar trend was also observed in cases **7** and **9** upon Soret band excitation and a faster decay/recovery of their ESA/GSB signals compared to that of **C1** corresponds to the formation of CS state in polar benzonitrile. Finally, CR from the CS state leads to the formation of triplets of these compounds, as also evident from the long-lived nature of the ESA signals peaking at ~ 500, 550, 580, 630, and 680 nm, having lifetime beyond the experimental time window of our TA setup. Subsequently, to understand the spectral and temporal behavior of the evolved photoexcited states, the TA data was subjected to target analysis[60] using a three-component fitting model (S_1 → CS → T_1) representing decay pathways of the photoinduced species. Figure 6 (right) displays the decay-associated spectra (DAS) of **5**, **7**, and **9**, respectively, obtained after target analysis; their associated time constants are also summarized in Table 3. The first DAS corresponds to the singlet excited state for all three compounds, while the second component suggests features of the CS state, as exemplified by the strong peak at 450-490 nm and the positive peaks spanning across the 500-700 nm region.[13-24] The lifetimes of the CS states of **5**, **7**, and **9** were found to be 235.97, 254.22, and 270.37 ps, respectively, after target analysis (Table 3), which subsequently relaxes to triplets of the respective compounds, represented by the third DAS which matches well with that of the strong positive peak in the 500 nm range, indicative of the formation of triplet excited states having lifetimes of >3 ns.[49] This follows the constructed energy level diagram of the respective compounds exhibiting singlet to long-lived triplet transitions *via* an intermediate of $MP^{\bullet-}$-$D^{\bullet+}$ CS state species. A similar trend in TA spectral characteristics was also identified in the case of **6**, **8**, and **10**, with their fs-TA spectra and related DAS after target analysis shown in Figure S37. Quite expected, these ZnP-D systems exhibited a slightly faster decay and recovery of the TA spectral feature when compared to that of the secondary donor-free **C2** reported in our previous work,[34] thus inhibiting CS upon photoexcitation. It is noteworthy that faster CS kinetics (Table 3) were observed in ZnP-D (**6**, **8**, and **10**) compared to their H_2P analogs (**5**, **7**, and **9**), likely due to the electronic influence by the central metal facilitating CS in the former systems. Likewise, a three-component S_1 → CS → T_1 fitting model truly justified the decay events of the photoinduced

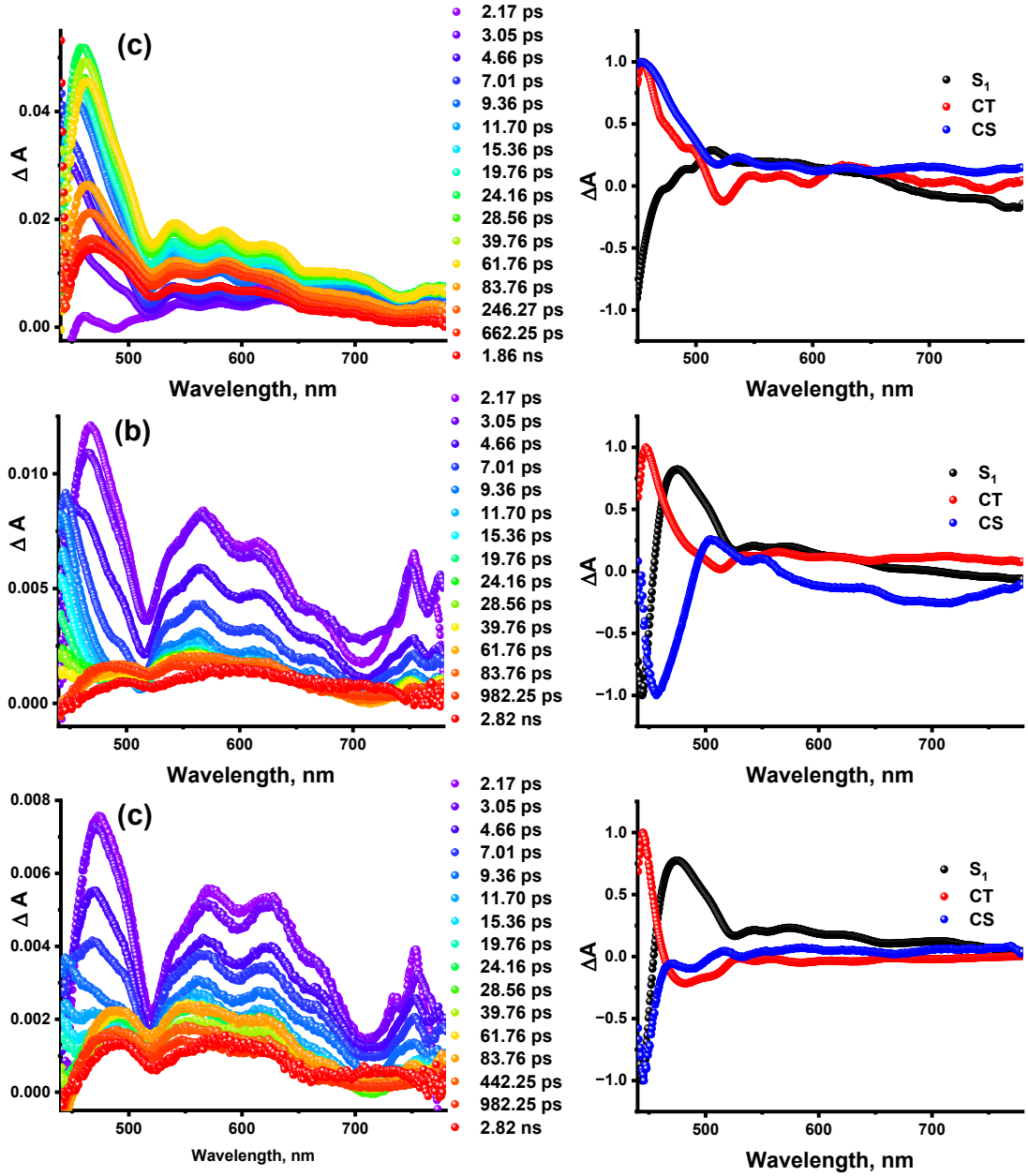

***Figure** 7. Fs-TA spectra at the indicated delay times of (a) **15**, (b) **17**, and (c) **19** in benzonitrile (λ_{ex} = 436 nm) are shown in the left column. Decay associated spectra from Target analysis are shown in the right column for **15**, **17**, and **19**, respectively.*

transients in **6**, **8,** and **10** with their associated time constants summarized in Table 3 and the related DAS provided in Figure S37.

Subsequently, fs-TA studies of the TCBD-incorporated H_2P-A-D and ZnP-A-D systems, **15-19**, were carried out by exciting the compounds related to their Soret band absorption with the

characteristic TA spectra summarized in Figure 7 for **15**, **17**, and **19**, and in Figure S38 for **16** and **18**. Following the steady-state absorption, the GSB signals of **15**, **17**, and **19** are found to be less intense (Figure 7, left panel), unlike their respective TCBD-free counterparts, shown earlier (Figure 6), suggesting ultrafast transition of singlets into corresponding CT states induced by the strong electron-deficient TCBD entity leading to the formation of $MP^{\delta+}$-$A^{\delta-}$-D species within 11-12 ps. Implementing a three-component fitting model ($S_1 \rightarrow CT \rightarrow CS$), as directed by the energy level diagram of these compounds, we have assessed the DAS and time constants related to the different photoinduced species, shown in Figure 7 (right). These rate constants of the transient species obtained from target analysis for both systems, MP-D and MP-A-D in benzonitrile, have been summarized in Table 3. Note that, in **15**, **17**, and **19**, the facile CT forms CS species stabilized by polar benzonitrile with a time constant of ~ 49-63 ps (Table 3). Interestingly, the lifetime of the CS states in **15**, **17**, and **19** are found to be much less compared to their analogous TCBD-free compounds (**5**, **7**, and **9**), indicating strong nonradiative transition operates in these systems, exhibiting CR from CS states leading to direct ground state deactivation of the photoinduced species. It is noteworthy that, due to greater Gibbs free energy change, singlet to CT transitions

Table 3. *Time constants obtained from Target analysis of the fs-TA data for different photo-events of the studied compounds in benzonitrile.*

Compound	λ_{ex}, nm	Solvent	S_1, ps	CT, ps	CS, ps	T_1, ns
5	428	PhCN	16.73	--	235.97	> 3
6	437		13.66	--	229.08	> 3
15	433		0.40	11.63	49.31	--
16	435		0.49	11.21	45.10	--
7	426	PhCN	0.44	--	254.22	> 3
8	438		2.68	--	244.08	> 3
17	430		1.15	12.13	60.08	--
18	438		2.63	11.90	55.09	--
9	424	PhCN	0.40	--	270.37	> 3
10	440		0.81	--	260.53	> 3
19	429		5.46	12.49	63.17	--

without involving the intermediate triplet (^{3}MP*) states (*via* ISC) are more favourable in the TCBD-incorporated samples, which, in turn, causes a more pronounced CT (as also evident from ground state absorption data) and, subsequently, a much faster CR to the ground state from the CS species. A much faster decay of the ESA in compounds **15**, **17**, **19** relative to **5**, **7**, and **9** (see spectra of longer delay times) also corroborates the non-association of ^{3}MP* in the former systems. A faster CS in the case of **16** and **18** compared to **6**, and **8** also suggests a similar deactivation scenario after TCBD incorporation, even in the case of ZnP-A-D systems (Figure S38 and Table 3).

It is important to note that, lower oxidation potential of the secondary donor entities compared to porphyrin core along with facile reduction of the TCBD moieties constitute a faster CT and subsequent CS events in the MP-A-D systems as evident from their respective lifetimes in Table 1. However, among all the secondary donor entities considered in this report, as well as the previous one,[34] Cz was found to provide better stabilization of the CS states in both MP-D and MP-A-D systems, which is evident from the longer CS time constants in **9**, **10**, and **19**, respectively, when compared to the other systems having different secondary donors (Table 3). Similarly, for the TCBD-based systems exhibiting CT states, a relatively longer CT lifetime was found in **9** with Cz as the secondary donor. A facile CS and longer CT/CS lifetime of all the systems upon photoexcitation, particularly for the Cz-containing MP-D and MP-A-D complexes, are expected to help develop efficient solar energy conversion and associated photonic devices comprising these materials.

Conclusions

To conclude, a new set of donor-substituted H_2P and ZnP based *β*-porphyrins (**5-10**) and their corresponding strong electron-deficient TCBD-functionalized counterparts (**15-19**) have been designed and successfully synthesized by Sonogashira cross-coupling followed by [2+2] CA–RE reactions. Steady-state optical studies revealed facile CT interactions across all the TCBD-embedded compounds, resulting in an additional low-energy absorption band extendable over 800 nm of the electromagnetic spectrum. While the electrochemical data corroborate feasibility of CT events, the computational studies, on the other hand, shed light on the molecular orbitals involved in excited state photo processes, which, in turn, suggested the formation of the energetically feasible MP$^{\bullet-}$-D$^{\bullet+}$ or MP$^{\bullet+}$-A$^{\bullet-}$-D type CS species in polar media, thus, switching the electronic

behavior of porphyrin core (acceptor to donor) towards CT transitions in the absence and presence of the TCBD acceptor. Finally, ultrafast fs-TA studies coupled with target analysis of the transient data provided spectral and temporal characteristics of the evolved photoinduced species for both the MP-D and MP-A-D systems and identified Cz to be the best secondary donor among the present set of donor entities in stabilizing CS state (with higher lifetimes) of these β-substituted porphyrins exhibiting facile CT and CS events. A broad absorption spanning across the visible window along with easy formation of long-lived CS states in these compounds make them coveted in utilizing advanced photovoltaic and related solar energy conversion applications.

Associated Content

Supporting Information

The supporting information contains ^{1}H NMR, ^{13}C NMR, and HRMS data, additional absorption, emission, and time-resolved fluorescence data, CVs of the compounds, an energy profile diagram, additional TA spectra, and related GTA fitting data, and a table of theoretical, electrochemistry, and TA results.

Author Information

Corresponding Authors

Rajneesh Misra - *Department of Chemistry, Indian Institute of Technology, Indore 453552, India*; E-mail: rajneeshmisra@iiti.ac.in

Francis D'Souza - *Department of Chemistry, University of North Texas, 1155 Union Circle, #305070, Denton, TX 76203-5017, United States*; E-mail: Francis.DSouza@UNT.edu; orcid.org/0000-0003-3815-8949

Authors

Andrew W. Dawson - *Department of Chemistry, University of North Texas, 1155 Union Circle, #305070, Denton, TX 76203-5017, United States*

Bijesh Sekaran - *Department of Chemistry, Indian Institute of Technology, Indore 453552, India*

Somnath Das - *Department of Chemistry, University of North Texas, 1155 Union Circle, #305070, Denton, TX 76203-5017, United States*

Author Contribution

A.W.D. and B.S. contributed equally to this work.

Conflict of Interest

There are no conflicts to declare.

Acknowledgment

We gratefully acknowledge support from the US-National Science Foundation (2345836 to FD), the Council of Scientific and Industrial Research (Project No. CSIR 01(2934)/18/EMR-II), New Delhi, SERB (Project No. CRG/2018/000032), New Delhi, Govt. of India. We also gratefully acknowledge the Sophisticated Instrumentation Centre (SIC), IIT Indore. B. S. thanks the Indian Institute of Technology (IIT), Indore, for the fellowship.

References

1. Ashraf, M.; Ayaz, M.; Khan, M.; Adil, S. F.; Farooq, W.; Ullah, N.; Tahir, M. N. Recent Trends in Sustainable Solar Energy Conversion Technologies: Mechanisms, Prospects, and Challenges. *Energy Fuels* **2023***, 37*, 6283-6301.
2. Hao, D.; Qi, L.; Tairab, A. M.; Ahmed, A.; Azam, A.; Luo, D.; Pan, Y.; Zhang, Z.; Yan, J. Solar energy harvesting technologies for PV self-powered applications: A comprehensive review. *Renewable Energy* **2022***, 188*, 678-697.
3. Armaroli, N.; Balzani, V. The Future of Energy Supply: Challenges and Opportunities. *Angew. Chem. Int. Ed.* **2007***, 46*, 52-66.
4. Mishra, A.; Bäuerle, P. Small Molecule Organic Semiconductors on the Move: Promises for Future Solar Energy Technology. *Angew. Chem. Int. Ed.* **2012***, 51*, 2020-2067.
5. Wang, Z.; Hu, Y.; Zhang, S.; Sun, Y. Artificial photosynthesis systems for solar energy conversion and storage: platforms and their realities. *Chem. Soc. Rev.* **2022***, 51*, 6704-6737.
6. Gust, D.; Moore, T. A.; Moore, A. L. Realizing artificial photosynthesis. *Faraday Discuss.* **2012***, 155*, 9-26.
7. D'Souza, F.; Ito, O. Photosensitized electron transfer processes of nanocarbons applicable to solar cells. *Chem. Soc. Rev.* **2012***, 41*, 86-96.
8. Gupta, P. K.; Das, S.; Misra, R.; D'Souza, F. Near-IR Capturing N-Methylbenzene Sulfonamide-Phenothiazine Incorporating Strong Electron Acceptor Push-Pull Systems: Photochemical Ultrafast Carrier Dynamics. *Chem. Eur. J.* **2024***, 30*, e202304313.

9. Alsaleh, A. Z.; Pinjari, D.; Das, S.; Misra, R.; D'Souza, F. Broad-Band-Capturing Tetracyanobutadiene-Incorporated Phenothiazine-azaBODIPY Push–Pull Systems: Excited State Charge Separation and Relaxation Dynamics. *J. Phys. Chem. C* **2024***, 128*, 7188-7201.

10. Das, S.; Rout, Y.; Poddar, M.; Alsaleh, A. Z.; Misra, R.; D'Souza, F. Novel Benzothiadiazole-based Donor-Acceptor Systems: Synthesis, Ultrafast Charge Transfer and Separation Dynamics. *Chem. Eur. J.* **2024***,* e202401959.

11. El-Khouly, M.; Fukuzumi, S.; D'Souza, F. Photosynthetic Antenna–Reaction Center Mimicry by Using Boron Dipyrromethene Sensitizers. *ChemPhysChem* **2014***, 15*, 30-47.

12. Bottari, G.; de la Torre, G.; Guldi, D. M.; Torres, T. Covalent and Noncovalent Phthalocyanine−Carbon Nanostructure Systems: Synthesis, Photoinduced Electron Transfer, and Application to Molecular Photovoltaics. *Chem. Rev.* **2010***, 110*, 6768-6816.

13. Gilbert, M.; Albinsson, B. Photoinduced charge and energy transfer in molecular wires. *Chem. Soc. Rev.* **2015***, 44*, 845-862.

14. Rohal, R. K.; Acharyya, J. N.; Shanu, M.; Prakash, G. V.; Sankar, M. β-Tetracyanobutadiene-Appended Porphyrins: Facile Synthesis, Spectral and Electrochemical Redox Properties, and Their Utilization as Excellent Optical Limiters. *Inorg. Chem.* **2022***, 61*, 1297-1307.

15. Bulbul, A. S.; Chaudhri, N.; Shanu, M.; Acharyya, J. N.; Prakash, G. V.; Sankar, M. Unsymmetrically β-Functionalized π-Extended Porphyrins: Synthesis, Spectral, Electrochemical Redox Properties, and Their Utilization as Efficient Two-Photon Absorbers. *Inorg. Chem.* **2022***, 61*, 9968-9982.

16. Yadav, I.; Osterloh, W. R.; Kadish, K. M.; Sankar, M. Synthesis, Spectral, Redox, and Sensing Studies of β-Dicyanovinyl-Appended Corroles and Their Metal Complexes. *Inorg. Chem.* **2023***, 62*, 7738-7752.

17. Yadav, I.; Sankar, M. Panchromatic and Perturbed Absorption Spectral Features and Multiredox Properties of Dicyanovinyl- and Dicyanobutadienyl-Appended Cobalt Corroles. *Inorg. Chem.* **2023***, 62*, 19956-19970.

18. Winterfeld, K. A.; Lavarda, G.; Guilleme, J.; Guldi, D. M.; Torres, T.; Bottari, G. Subphthalocyanine–tetracyanobuta-1,3-diene–aniline conjugates: stereoisomerism and photophysical properties. *Chem. Sci.* **2019***, 10*, 10997-11005.

19. Tancini, F.; Monti, F.; Howes, K.; Belbakra, A.; Listorti, A.; Schweizer, W. B.; Reutenauer, P.; Alonso-Gómez, J.; Chiorboli, C.; Urner, L. M.; *et al.* Cyanobuta-1,3-dienes as Novel Electron Acceptors for Photoactive Multicomponent Systems. *Chem. Eur. J.* **2014***, 20*, 202-216.

20. Wang, C.; Fan, C.; Yuan, C.; Yang, G.; Li, X.; Ju, C.; Feng, Y.; Xu, J. Third- and high-order nonlinear optical properties of an intramolecular charge-transfer compound. *RSC Adv.* **2017***, 7*, 4825-4829.

21. Dar, A. H.; Gowri, V.; Gopal, A.; Muthukrishnan, A.; Bajaj, A.; Sartaliya, S.; Selim, A.; Ali, M. E.; Jayamurugan, G. Designing of Push–Pull Chromophores with Tunable Electronic and

Luminescent Properties Using Urea as the Electron Donor. *J. Org. Chem.* **2019***, 84*, 8941-8947.

22. Erden, K.; Dengiz, C. 3-Alkynylindoles as Building Blocks for the Synthesis of Electronically Tunable Indole-Based Push–Pull Chromophores. *J. Org. Chem.* **2022***, 87*, 4385-4399.

23. Michinobu, T.; Diederich, F. The [2+2] Cycloaddition-Retroelectrocyclization (CA-RE) Click Reaction: Facile Access to Molecular and Polymeric Push-Pull Chromophores. *Angew. Chem. Int. Ed.* **2018***, 57*, 3552-3577.

24. Rao, P. S.; Brixi, S.; Shaikh, D. B.; Kobaisi, M. A.; Lessard, B. H.; Bhosale, S. V.; Bhosale, S. V. The Effect of TCNE and TCNQ Acceptor Units on Triphenylamine-Naphthalenediimide Push-Pull Chromophore Properties. *Eur. J. Org. Chem.* **2021***, 2021*, 2615-2624.

25. Li, Z.; Gong, Q.; Hao, E.; Jiao, L. B(III)-subporphyrazines, B(III)-subporphyrins and their hybrids. *Coord. Chem. Rev.* **2023***, 493*, 215325.

26. Ileperuma, C. V.; Garcés-Garcés, J.; Shao, S.; Fernández-Lázaro, F.; Sastre-Santos, Á; Karr, P. A.; D'Souza, F. Panchromatic Light-Capturing Bis-styryl BODIPY-Perylenediimide Donor-Acceptor Constructs: Occurrence of Sequential Energy Transfer Followed by Electron Transfer. *Chem. Eur. J.* **2023***, 29*, e202301686.

27. Jang, Y.; Rout, Y.; Misra, R.; D'Souza, F. Symmetric and Asymmetric Push–Pull Conjugates: Significance of Pull Group Strength on Charge Transfer and Separation. *J. Phys. Chem. B* **2021***, 125*, 4067-4075.

28. Khan, F.; Jang, Y.; Patil, Y.; Misra, R.; D'Souza, F. Photoinduced Charge Separation Prompted Intervalence Charge Transfer in a Bis(thienyl)diketopyrrolopyrrole Bridged Donor-TCBD Push-Pull System. *Angew. Chem. Int. Ed.* **2021***, 60*, 20518-20527.

29. Pinjari, D.; Alsaleh, A. Z.; Patil, Y.; Misra, R.; D'Souza, F. Interfacing High-Energy Charge-Transfer States to a Near-IR Sensitizer for Efficient Electron Transfer upon Near-IR Irradiation. *Angew. Chem. Int. Ed.* **2020***, 59*, 23697-23705.

30. Poddar, M.; Jang, Y.; Misra, R.; D'Souza, F. Excited-State Electron Transfer in 1,1,4,4-Tetracyanobuta-1,3-diene (TCBD)- and Cyclohexa-2,5-diene-1,4-diylidene-Expanded TCBD-Substituted BODIPY-Phenothiazine Donor–Acceptor Conjugates. *Chem. Eur. J.* **2020***, 26*, 6869-6878.

31. Yadav, I. S.; Alsaleh, A. Z.; Misra, R.; D'Souza, F. Charge stabilization via electron exchange: excited charge separation in symmetric, central triphenylamine derived, dimethylaminophenyl–tetracyanobutadiene donor–acceptor conjugates. *Chem. Sci.* **2021***, 12*, 1109-1120.

32. Yahagh, A.; Kaswan, R. R.; Kazemi, S.; Karr, P. A.; D'Souza, F. Symmetry breaking charge transfer leading to charge separation in a far-red absorbing bisstyryl-BODIPY dimer. *Chem. Sci.* **2024***, 15*, 906-913.

33. Sekita, M.; Ballesteros, B.; Diederich, F.; Guldi, D. M.; Bottari, G.; Torres, T. Intense Ground-State Charge-Transfer Interactions in Low-Bandgap, Panchromatic Phthalocyanine–Tetracyanobuta-1,3-diene Conjugates. *Angew. Chem. Int. Ed.* **2016***, 55*, 5560-5564.

34. Sekaran, B.; Dawson, A.; Jang, Y.; MohanSingh, K. V.; Misra, R.; D'Souza, F. Charge-Transfer in Panchromatic Porphyrin-Tetracyanobuta-1,3-Diene-Donor Conjugates: Switching the Role of Porphyrin in the Charge Separation Process. *Chem. Eur. J.* **2021***, 27*, 14335-14344.

35. Rout, Y.; Jang, Y.; Gobeze, H. B.; Misra, R.; D'Souza, F. Conversion of Large-Bandgap Triphenylamine–Benzothiadiazole to Low-Bandgap, Wide-Band Capturing Donor–Acceptor Systems by Tetracyanobutadiene and/or Dicyanoquinodimethane Insertion for Ultrafast Charge Separation. *J. Phys. Chem. C* **2019***, 123*, 23382-23389.

36. Yadav, I. S.; Alsaleh, A. Z.; Misra, R.; D'Souza, F. Charge stabilization via electron exchange: excited charge separation in symmetric, central triphenylamine derived, dimethylaminophenyl–tetracyanobutadiene donor–acceptor conjugates. *Chem. Sci.* **2021***, 12*, 1109-1120.

37. Jang, Y.; Sekaran, B.; Singh, P. P.; Misra, R.; D'Souza, F. Accelerated Intramolecular Charge Transfer in Tetracyanobutadiene- and Expanded Tetracyanobutadiene-Incorporated Asymmetric Triphenylamine–Quinoxaline Push–Pull Conjugates. *J. Phys. Chem. A* **2023***, 127*, 4455-4462.

38. Khan, F.; Jang, Y.; Patil, Y.; Misra, R.; D'Souza, F. Photoinduced Charge Separation Prompted Intervalence Charge Transfer in a Bis(thienyl)diketopyrrolopyrrole Bridged Donor-TCBD Push-Pull System. *Angew. Chem. Int. Ed.* **2021***, 60*, 20518-20527.

39. Guragain, M.; Pinjari, D.; Misra, R.; D'Souza, F. Zinc Tetrapyrrole Coordinated to Imidazole Functionalized Tetracyanobutadiene or Cyclohexa-2,5-diene-1,4-diylidene-expanded-tetracyanobutadiene Conjugates: Dark vs. Light-Induced Electron Transfer. *Chem. Eur. J.* **2023***, 29*, e202302665.

40. Sekaran, B.; Guragain, M.; Misra, R.; D'Souza, F. β-Pyrrole Functionalized Push or Pull Porphyrins: Excited Charge Transfer Promoted Singlet Oxygen Generation. *J. Phys. Chem. A* **2023***, 127*, 7964-7975.

41. Grover, N.; Chaudhri, N.; Sankar, M. β-substituted donor-acceptor porphyrins: Synthesis, energy transfer and electrochemical redox properties. *Dyes Pigm.* **2019***, 161*, 104-112.

42. Hiroto, S.; Miyake, Y.; Shinokubo, H. Synthesis and Functionalization of Porphyrins through Organometallic Methodologies. *Chem. Rev.* **2017***, 117*, 2910-3043.

43. Holzer, N.; Jin, J.; Nesterov, V. N.; Sharma, J. K.; Zarrabi, N.; D'Souza, F.; Poddutoori, P. K. Fluorinated Antimony(V) Tetraarylporphyrins as High-Valent Electron Acceptors with Unparalleled Reduction Potentials. *Inorg. Chem.* **2023***, 62*, 7097-7110.

44. Subedi, D. R.; Jang, Y.; Ganesan, A.; Schoellhorn, S.; Reid, R.; Verbeck, G. F.; D'Souza, F. Donor-acceptor conjugates derived from cobalt porphyrin and fullerene via metal-ligand axial coordination: Formation and excited state charge separation. *J. Porphyr. Phthalocyanines* **2021***, 25*, 533-546.

45. Guldi, D. M.; Fukuzumi, S. Electron transfer in electron donor-acceptor ensembles containing porphyrins and metalloporphyrins. *J. Porphyr. Phthalocyanines* **2002***, 06*, 289-295.

46. Kadish, K.; Smith, K. M.; Guilard, R. *The Porphyrin Handbook, Volume 3: Inorganic, Organometallic and Coordination Chemistry;* Academic Press, 2000.

47. Fukuzumi, S.; Honda, T.; Kojima, T. Structures and photoinduced electron transfer of protonated complexes of porphyrins and metallophthalocyanines. *Coord. Chem. Rev.* **2012***, 256*, 2488-2502.

48. KC, C. B.; D'Souza, F. Design and photochemical study of supramolecular donor–acceptor systems assembled via metal–ligand axial coordination. *Coord. Chem. Rev.* **2016***, 322*, 104-141.

49. Sekaran, B.; Jang, Y.; Misra, R.; D'Souza, F. Push–Pull Porphyrins via β-Pyrrole Functionalization: Evidence of Excited State Events Leading to High-Potential Charge-Separated States. *Chem. Eur. J.* **2019***, 25*, 12991-13001.

50. Zarrabi, N.; Seetharaman, S.; Chaudhuri, S.; Holzer, N.; Batista, V. S.; van der Est, A.; D'Souza, F.; Poddutoori, P. K. Decelerating Charge Recombination Using Fluorinated Porphyrins in N,N-Bis(3,4,5-trimethoxyphenyl)aniline—Aluminum(III) Porphyrin—Fullerene Reaction Center Models. *J. Am. Chem. Soc.* **2020***, 142*, 10008-10024.

51. Reekie, T. A.; Sekita, M.; Urner, L. M.; Bauroth, S.; Ruhlmann, L.; Gisselbrecht, J.; Boudon, C.; Trapp, N.; Clark, T.; Guldi, D. M.; *et al.* Porphyrin Donor and Tunable Push–Pull Acceptor Conjugates—Experimental Investigation of Marcus Theory. *Chem. Eur. J.* **2017***, 23*, 6357-6369.

52. Beaujuge, P. M.; Fréchet, J. M. J. Molecular Design and Ordering Effects in π-Functional Materials for Transistor and Solar Cell Applications. *J. Am. Chem. Soc.* **2011***, 133*, 20009-20029.

53. Bijesh, S.; Misra, R. Triphenylamine Functionalized Unsymmetrical Quinoxalines. *Asian J. Org. Chem.* **2018***, 7*, 1882-1892.

54. Yeung, M.; Ng, A. C. H.; Drew, M. G. B.; Vorpagel, E.; Breitung, E. M.; McMahon, R. J.; Ng, D. K. P. Facile Synthesis and Nonlinear Optical Properties of Push−Pull 5,15-Diphenylporphyrins. *J. Org. Chem.* **1998***, 63*, 7143-7150.

55. Gao, G.; Ruppel, J. V.; Allen, D. B.; Chen, Y.; Zhang, X. P. Synthesis of β-Functionalized Porphyrins via Palladium-Catalyzed Carbon−Heteroatom Bond Formations: Expedient Entry into β-Chiral Porphyrins. *J. Org. Chem.* **2007***, 72*, 9060-9066.

56. Fukuzumi, S.; Kotani, H.; Ohkubo, K.; Ogo, S.; Tkachenko, N. V.; Lemmetyinen, H. Electron-Transfer State of 9-Mesityl-10-methylacridinium Ion with a Much Longer Lifetime and Higher Energy Than That of the Natural Photosynthetic Reaction Center. *J. Am. Chem. Soc.* **2004***, 126*, 1600-1601.

57. Kivala, M.; Boudon, C.; Gisselbrecht, J.; Seiler, P.; Gross, M.; Diederich, F. Charge-Transfer Chromophores by Cycloaddition–Retro-electrocyclization: Multivalent Systems and Cascade Reactions. *Angew. Chem. Int. Ed.* **2007***, 46*, 6357-6360.

58. Frisch, M. J.; Trucks, G. W.; Schlegel, H. B.; Scuseria, G. E.; Robb, M. A.; Cheeseman, J. R.; Scalmani, G.; Barone, V.; Mennucci, B.; Petersson, G. A.; *et al. Gaussian 09, Revision B.01*. Gaussian, Inc.; Wallingford, CT. **2010**.

59. Rehm, D.; Weller, A. Kinetics of Fluorescence Quenching by Electron and H-Atom Transfer. *Isr. J. Chem.* **1970***, 8*, 259-271.

60. Snellenburg, J. J.; Laptenok, S.; Seger, R.; Mullen, K. M.; van Stokkum, I. H. M. Glotaran: A Java-Based Graphical User Interface for the R Package TIMP. *J. Stat. Softw.* **2012**, *49*, 1– 22.

Entry for the Table of Contents